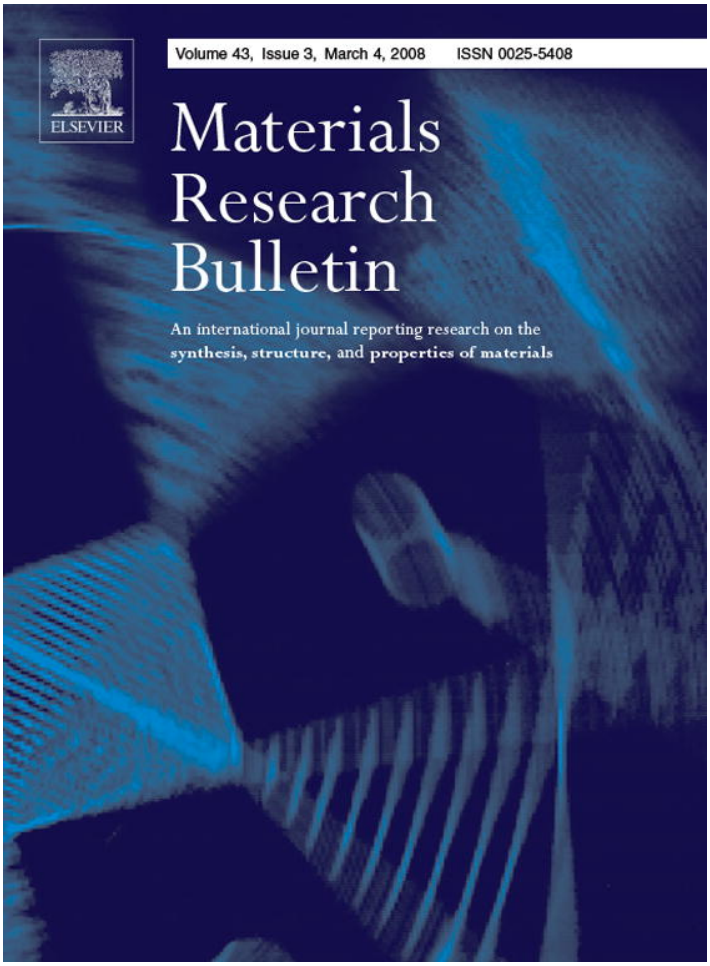

Available online at www.sciencedirect.com
ScienceDirect
Materials Research Bulletin 43 (2008) 561–571
Materials Research Bulletin
www.elsevier.com/locate/matresbu

Phase development in the hardening process of two calcium phosphate bone cements: an energy dispersive X-ray diffraction study

A. Generosi [a], V.V. Smirnov [b], J.V. Rau [c], V. Rossi Albertini [a], D. Ferro [c], S.M. Barinov [b,*]

[a] *Istituto di Struttura della Materia, CNR, via del Fosso del Cavaliere, 100-00133 Rome, Italy*
[b] *Institute for Physical Chemistry of Ceramics, Russian Academy of Sciences, Ozernaya 48, Moscow 119361, Russia*
[c] *Istituto per lo Studio dei Materiali Nanostrutturati, CNR, Piazzale Aldo Moro, 5-00185 Rome, Italy*

Received 14 March 2007; accepted 9 April 2007
Available online 19 April 2007

Abstract

This work was aimed at the application of an energy dispersive X-ray diffraction technique to study the kinetics of phase development during the setting and hardening reactions in two calcium phosphate bone cements. The cements under study are based on either tricalcium phosphate or tetracalcium phosphate initial solid phase, and a magnesium carbonate–phosphoric acid liquid phase as the hardening liquid. The application of the energy dispersive X-ray diffraction method allowed to collect the diffraction patterns from the cement pastes *in situ* starting from 1 min of the setting and hardening process. The only crystallized phase in both cements was apatite-like phase, the primary crystallization process proceeds during a few seconds of the setting reaction. Both the compressive strength and the pH value changes during the hardening period can be attributed to the transformations occurring in the intergranular X-ray amorphous phase.

Keywords: A. Ceramics; B. Chemical synthesis; C. X-ray diffraction

1. Introduction

Calcium phosphate materials have found many applications as biomaterials for bone substitution and repair [1,2]. Mostly, the calcium phosphate materials are used in the form of sintered ceramic blocks or granules. However, the incorporation of blocks may be limited due to defect geometry leading to incomplete bone-implant contact and, thus, to insufficient osteointegration [3]. Granules risk migrating from the original defect [3]. The invention of calcium phosphate cements (CPC) resulted in a new family of bone substitute materials [4–7]. The common property of this class of biomaterials is that, after mixing of one or several calcium phosphate powders and a liquid phase, they turn into a pasty, moldable compound that sets to a firm mass at physiological temperature [3,4–8]. A considerable effort and a large number of studies have been devoted to CPCs, the most recent technological issues for the development of efficient CPCs being assessed in a review [9]. Despite the relatively long history of CPCs, since 1982 [10], presently

* Corresponding author. Tel.: +7 495 4379892; fax: +7 495 4379893.
E-mail address: barinov_s@mail.ru (S.M. Barinov).

0025-5408/$ – see front matter © 2007 Elsevier Ltd. All rights reserved.
doi:10.1016/j.materresbull.2007.04.016

little is known about some basic properties of CPCs, such as the setting behavior and hardening mechanism [9]. This is rather surprising because the phase development in the hardening process influences the mechanical properties, setting time and interaction of the CPC with surrounding environment, e.g. blood.

Two types of CPCs can be distinguished in accordance to the main product of chemical interaction during the setting reaction: deposited apatite (DAP, calcium orthophosphate of general formula $Ca_{10-x}(HPO_4)_x(PO_4)_{6-x}(OH)_{2-x}$, Ca/P = 1.50–1.67) and dicalcium phosphate dihydrate (DCPD, $CaHPO_4{\cdot}2H_2O$, Ca/P = 1.0) [6]. These two phases are often presented simultaneously as the setting reaction products in the cement. As DCPD is a metastable compound, it turns into hydroxyapatite under physiological conditions [11]. An example of the dynamics for the hydraulic process in a CPC is the X-ray diffraction (XRD) study reported in [12]. The hardening process was found to be controlled initially by the dissolution of reactants (tetracalcium phosphate (basic compound, Ca/P = 2.0) and dicalcium phosphate (acidic compound, Ca/P = 1.0)), followed by the precipitation of DAP around the reactants. The precipitate consists of small petal-like or needle-like crystals, which are responsible for the adherence of grains resulting in hardening. A maximum compressive strength (51 MPa) was found to be tolerable by the sample at this stage of the hardening process. Further conversion of the reactants into the DAP resulted in a decrease of the compressive strength due to the final reaction product, acircular DAP particles [12]. Those results illustrate the importance of phase development monitoring to control the properties of the CPC. The fracture strength of the common CPCs is generally modest [3–6], and research should be focused on improving the strength.

The XRD has always been the main technique to study the phase development in powder samples. However, common laboratory XRD measurements can be little suitable and too slow to monitor rapid phase transformations occurring in the CPC system during the setting and hardening processes. To address problems analogous to the present one, an alternative method, the energy dispersive X-ray diffraction (EDXD), has been developed [13,14]. This method consists of irradiating the sample by a non-monochromatized X-ray beam, keeping the scattering angle unchanged. The diffraction pattern is collected through the measurement of the energy spectrum of such polychromatic beam after it is scattered by the sample. EDXD makes use of the instruments similar to those used in the ordinary X-ray fluorescence spectroscopy, the difference being that the spectrum provides structural information rather than spectroscopic ones. The advantage of EDXD is that no movement is needed during the data collection, which makes the procedure of analysis much more reliable than that for the common XRD. Indeed, since the diffraction geometry (i.e. irradiated volume and surface) remains unchanged during the measurement, no problems coming from renormalization or from irradiation of different parts of the sample at different angles occur. Such problems are particularly serious when inhomogeneous samples are studied and/or when time resolved measurements, which require the collections of many diffraction patterns, are carried out. The EDXD method and apparatus have been described in details elsewhere [13–15].

The present study is aimed to the use of the EDXD technique to investigate the phase development in two different novel CPCs.

2. Experimental

2.1. Materials preparation and characterization

Two different CPCs were prepared. Cement 1 is based on alpha tricalcium phosphate (α-TCP) powder. The initial amorphous phosphate has been obtained as the precipitation product of the reaction

$$3Ca(NO_3)_2 + 2(NH_4)_2HPO_4 + 2NH_4OH + nH_2O \rightarrow Ca_3(PO_4)_2{\cdot}nH_2O + 6NH_4NO_3 + 2H_2O$$

Analytical grade starting reagents were used. The solution pH was adjusted to 7 by adding solutions of acetic acid and ammonia. The solution with the precipitate was aged for 24 h, followed by filtering with a Buechner cone filter. After the calcinations of the precipitate in an air atmosphere furnace at 1300 °C for 1 h, the monophase α-TCP powder was obtained, as established by XRD analysis (diffractometer Shimadzu XRD-6000, Cu Kα radiation, JCPDS data base). The powders were milled to a mean particle size of about 10 μm.

Cement 2 was based on tetracalcium phosphate (TetCP, $Ca_4P_2O_9$) powder. The initial reagents, calcium oxide and solid ammonium hydrophosphate, were mixed in a planetary ball mill for 30 min using alumina balls. After that, the mix was submitted to a heat treatment at 1500 °C for 1 h in an air furnace to initiate the following reaction

$$4CaO + 2(NH_4)_2HPO_4 \rightarrow Ca_4P_2O_9 + NH_3 + 3NH_4OH$$

The reaction product, a white powder, was milled in a ball mill to the mean particle size of 10 μm. XRD analysis showed the powder is TetCP containing minor amount of hydroxyapatite (about 3 wt.%, determined using a calibration curve) as an impurity phase.

To obtain the cement pastes, two liquids were prepared by the following routes. The liquid for the cement 1 was prepared mixing of 0.15 g of magnesium carbonate, $MgCO_3$, with 0.18 ml of diluted H_3PO_4. The same procedure was employed for cement 2, but with 0.22 ml of acid. Magnesium carbonate interacts with phosphoric acid, the reaction product being an aqueous solution of magnesium phosphates of varying Mg/PO_4 which depends on the initial reagents ratio. To prepare the cement samples, the powders of α-TCP and TetCP were added to the respective liquids, and mixed intensively with a spatula on plate glass to produce homogeneous cream-like pastes. The pastes were poured into PTFE plastic moulds 6 mm in diameter and 10 mm in height and held in an isotonic 0.9% NaCl solution for injections. The samples were further held in a thermostatic furnace at 37 °C and 100% relative humidity. Setting time of the pastes was evaluated by using a 1-mm tip diameter Vicat needle meter with 400-g load (according to ISO standard 1566). The cement is considered set when the needle fails to make a perceptible circular indentation on the surface of the cement. The pH measurements were performed as follows. Samples (1 g) of crushed cement after 0.5–10 days of sustaining in an isotonic solution were placed into a 50 ml volume flask, and distilled water was added to a 50 ml volume. pH value was measured after a 30 min soaking time using a Hanna Instruments HI 8314 pH meter. The compressive strength was determined using a stiff UTS-100 universal testing machine at the deformation speed of 0.1 mm/min.

2.2. EDXD measurements

An X-ray diffraction pattern represents the intensity of the X-ray radiation elastically scattered by a sample as a function of the momentum transfer Δq. The momentum transfer amplitude takes the name of scattering parameter: $q(E, \vartheta) = aE \sin \vartheta$, E being the energy of the electromagnetic radiation, 2ϑ the scattering angle and a = constant = 1.014 $Å^{-1}$/keV [15]. To perform the reciprocal space scan, namely to collect a diffraction pattern, two modes are thus available. The first, most conventional, consists of monochromatising the X-ray radiation (selecting a single energy component) and carrying out an angular scan by the mechanical movement of the arms of the diffractometer (Angular Dispersive Mode ADXD). Alternatively, an X-ray white beam can be used, fixing the angle 2ϑ (energy dispersive EDXD) executing the reciprocal space scan electronically. In this case, a solid state detector (SSD) is utilized. The SSD is able to detect not only the number of photons diffracted by the sample, but the energy of each of them, too. The latter mode was chosen to perform the measurements reported below, due to the intrinsic advantages on the ADXD counterpart. Among them, the simpler geometric arrangement, no movement being required during the measurement. This feature prevents any systematic error that can affect the AD measurements, due to the variation of the scattering volume during the angular scan. Furthermore, since a parallel collection of the experimental points at the various q-values takes place in the ED mode, the acquisition time is much reduced.

The ED diffractometer is a non commercial apparatus [15], very simple from the mechanical point of view. It consists of two arms pivoting around the optical centre of the instrument, where the sample holder is located. A white X-ray radiation is produced by a commercial W-anode X-ray tube (12–55 keV) and is collimated upstream and downhill the sample by four W slits. The detection is accomplished by an EG & G high purity germanium SSD. The detector is connected to a PC via ADCAM hardware and the signal is processed by a Maestro software, which performs the necessary analogue to digital conversions. Neither monochromator nor goniometer is required in the energy dispersive mode.

3. Results and discussion

3.1. EDXD data

3.1.1. Ex-situ measurements

Series of EDXD measurements were performed as preliminary tests on the pristine powders for cements 1 and 2, respectively. Several diffraction patterns were collected at various scattering angles, in order to make a wide q-scan and, therefore individuate the q-region of interest. Indeed, according to the previous expression for q, keeping the maximum beam energy fixed to 55 keV and progressively increasing the scattering angle 2ϑ, the sequence of Bragg

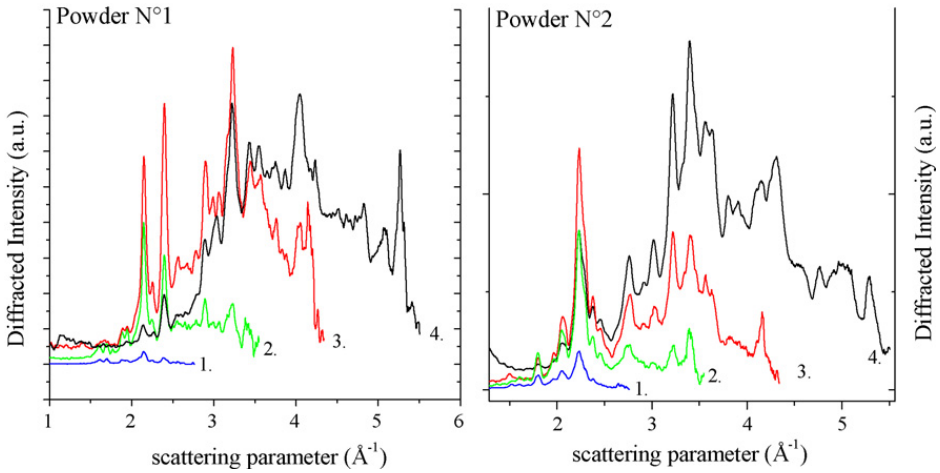

Fig. 1. Diffraction patterns collected upon powder no. 1 and no. 2 at different scattering angles: line 1, $\vartheta = 2.7°$; line 2, $\vartheta = 3.4°$; line 3, $\vartheta = 4.2°$; line 4, $\vartheta = 5.3°$.

peaks in the q-range (0.5, 5.5) $Å^{-1}$ could be detected. In Fig. 1, the raw data collected at the various diffraction angles are shown. They are not normalized, since the aim was to find out the diffraction features in the various zones of the reciprocal space, only.

By chance, in the present case, the pattern collected at the highest angle includes all the structural information contained in those acquired at lower angles. Therefore, the diffraction angle was set at $\vartheta = 5.3°$ and the corresponding pattern was normalized and refined properly, as shown in Fig. 2. The circle visible in Fig. 2(a) and covering two peaks, corresponds to an echo, a well known detector effect, which produces spurious signals. The peaks assignment was made by comparison with powder diffraction data taken from the literature. As expected, the result of the comparison confirmed the powder was $Ca_3(PO_4)_2$, as already established by preliminary measurements performed by using the conventional technique.

Powder 2, nominally being $Ca_4P_2O_9$, matched with published data (although the assignment of the Miller indexes to each Bragg peak was not found in literature).

Starting from these precursor powders, two different cements (cement 1 starting from the $Ca_3(PO_4)_2$ powder and cement 2 starting from the $Ca_4P_2O_9$ one) were produced ex-situ and characterized by EDXD measurements. Diffraction patterns were collected at the same angle mentioned before ($\vartheta = 5.3°$).

Regardless the starting powder, similar phase composition of final cements was revealed, their diffraction patterns being substantially overlapping (Fig. 3). The final crystalline structure could be attributed to the formation of

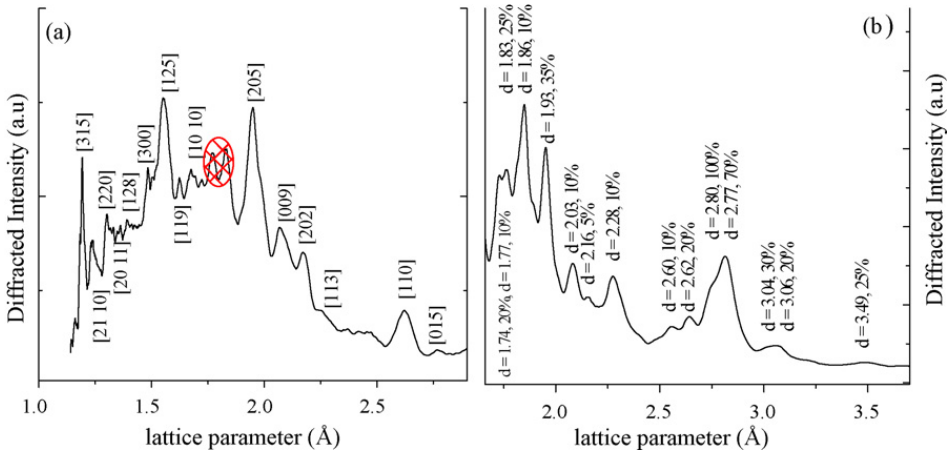

Fig. 2. Diffraction patterns of (a) $Ca_3(PO_4)_2$ and (b) $Ca_4P_2O_9$ powders, collected at $\vartheta = 5.331°$ and $\vartheta = 3.433°$ respectively.(a) The attribution of the Miller index is made. (b) The intermolecular lattice distances only could be calculated, while the relative intensity of each peak was taken from literature (® 2000 JCPDS-International Centre for Diffraction Data. All rights reserved. PCPDFWIN v 2.1).

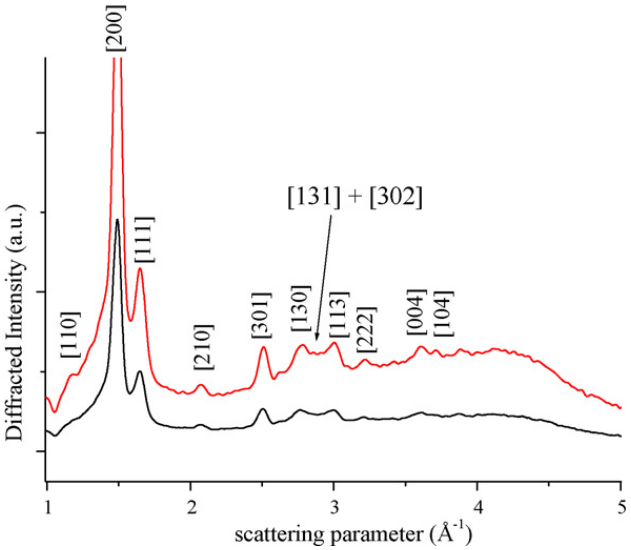

Fig. 3. Diffraction patterns collected at $\vartheta = 5.3^\circ$ on cement no. 1 (upper line) and cement no. 2 (lower line).

hydroxyapatite, $Ca_{10}(PO_4)_6(OH)_2$, with an hexagonal lattice (space group $P6_3/m$). In Fig. 3, the Miller indexes are assigned (cement 1, upper line, and cement 2, lower line). In Fig. 4, an overall comparison among the starting powders patterns ($Ca_3(PO_4)_2$–line 1, $Ca_4P_2O_9$–line 2.) and the final cement structure ($Ca_{10}(PO_4)_6(OH)_2$–line 3), all collected at $\vartheta = 5.3^\circ$, is shown. Moreover, line 4 represents the scattering contribution due to the sample holder, which is visibly negligible. The hollow circle drawn in the (1–2)$Å^{-1}$ q-range, includes the region where the structural differences between the precursor powders and the final cement are most evident. This region corresponds to the q-range spanned by setting the diffraction angle to 2.7°, as shown in the inset of Fig. 4. Indeed, at such scattering angle, the structural differences between powder 1 (line 1), powder 2 (line 2) and the final cement (line 3) are enhanced. The sampling in this reduced zone of reciprocal space, being the diffracted intensity much higher, is more accurate. To summarise, thanks to an initial wide exploration of the q-space carried out at 5.3°, the diffractometric region of interest for the cement formation was found to correspond to a diffraction angle $\vartheta = 2.7^\circ$. As a consequence, the *in situ* measurements were performed at the latter angle.

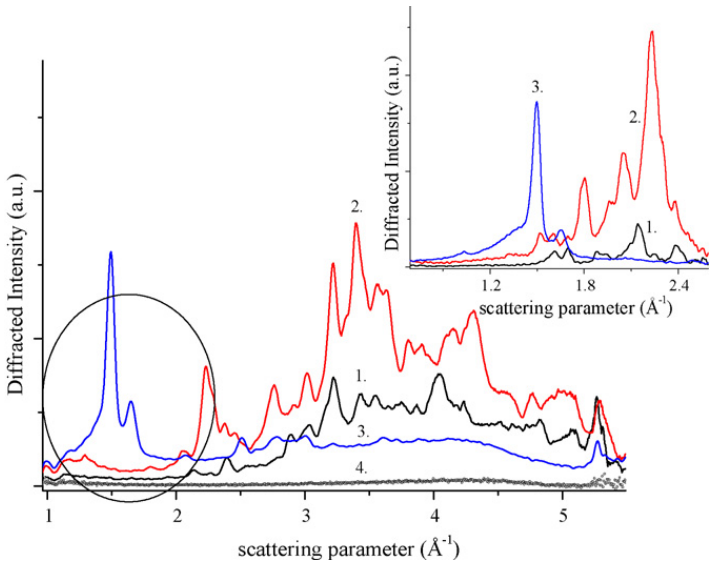

Fig. 4. Comparison of EDXD patterns collected at $\vartheta = 5.3^\circ$ upon $Ca_3(PO_4)_2$ (line 1), $Ca_4P_2O_9$ (line 2) and $Ca_{10}(PO_4)(OH)_2$ (line 3). Line 4 represents the sample holder contribution. In the inset the same comparison is shown ($\vartheta = 2.7^\circ$) in the q-range where the structural differences are most evident.

3.1.2. In situ *measurements*

The higher diffraction intensity attainable at the angle selected $\vartheta = 2.7^{\circ}$, coupled with the huge structural differences between the precursor powders and the final product, allowed to reduce the acquisition times in the region of interest in comparison to those required if higher scattering angles had been used. Starting from these preliminary considerations, *in situ* time resolved EDXD measurements were accomplished in order to study the crystallization process starting from the precursors until the final product was obtained. They consisted of collecting a sequence of diffraction pattern at a fixed angle in order to describe the structural rearrangement of the sample upon crystallization.

Cement 1 and cement 2 were prepared *in situ* and diffraction patterns were collected after 1, 5, 8, 12, 20 min and, then, every hour for 72 h. In this way, it was possible both to detect the crystallization process at the early stages of the setting reaction and to observe the slower secondary crystallization over a larger time scale.

In Fig. 5, the sequence of diffraction patterns collected during the crystallization of cement 1 (a) and cement 2 (b) are shown as a function of the scattering parameter and of time and, in Fig. 6, the spectrum collected during the first 20 min is compared with those obtained after several hours. As can be seen, the first spectrum collected during the initial 60 s of the interaction of powder 1 and powder 2 with the liquid, already exhibits the spectral profile characterizing the final cement. Even in these first patterns, no trace remains of reflections of either $Ca_3(PO_4)_2$ or $Ca_4P_2O_9$ (in Fig. 6a and b, respectively). This means that the reaction between each precursor and the liquid is very fast, i.e. faster than a few seconds. Indeed, if the crystallization process to obtain the final structure attributed to the cement lasted some seconds (say n seconds), in an acquisition time of 60 s, the pattern would exhibit peaks having an amplitude equal to $n/60$ of that corresponding to precursors reflections. Therefore, taking into account the statistical noise and since no trace of these reflection is visible already in the second diffraction pattern, we can affirm that the transition to the cement phase takes place in less than 1–2 s. As a consequence, our analysis was concentrated on longer times, namely on the secondary process. As evidenced by the hollow circles in Fig. 6a and b, after several hours from the beginning of the crystallization, the appearance of new Bragg reflections ([2 1 0] and [3 0 1]) could actually be observed. This is the clue of the occurrence of a secondary crystallization. From the analysis of the relative intensities variation of these peaks, the characteristic times of the secondary process were obtained.

In fact, examining at first the behaviour of the precursor powder α-$Ca_3(PO_4)_2$, the time evolution of both Bragg reflections mentioned above could be easy followed and their growth monitored as shown in Fig. 7. The appearance of the [2 1 0] and [3 0 1] reflections is simultaneous and their growth can be fitted by two Boltzmann curves (Fig. 7A, continuous line), having the same characteristic time $\tau_1 = (23 \pm 1)$ hours. Also the [2 0 0] and [1 1 1] reflection

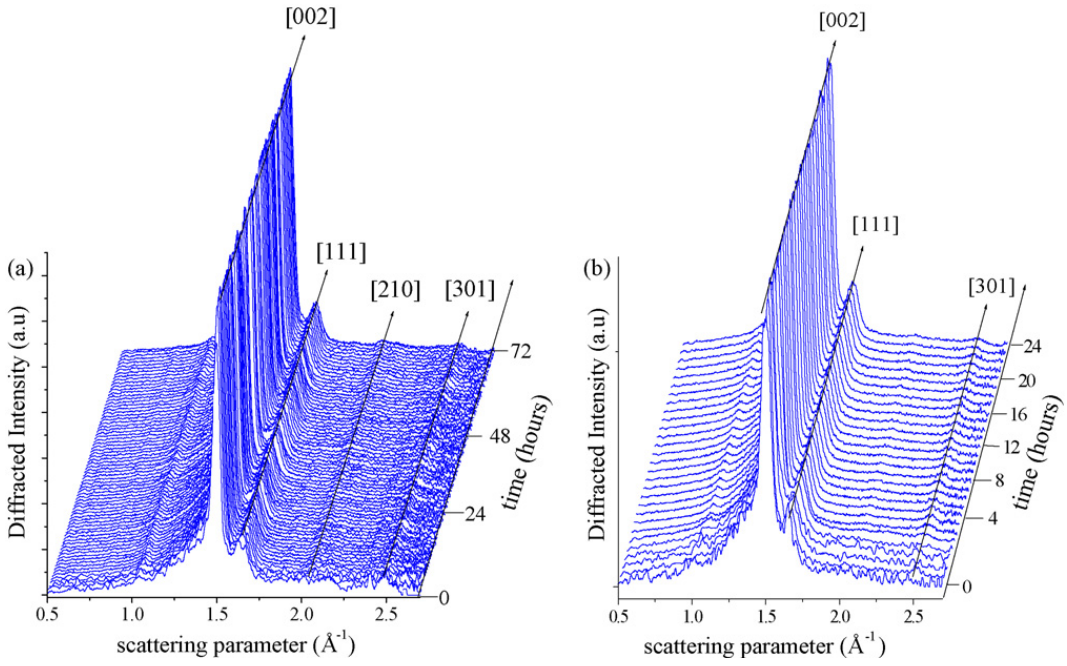

Fig. 5. Sequences of EDXD patterns collected as a function of the scattering parameter and of time during the crystallization process of cement 1 (a) and cement 2 (b).

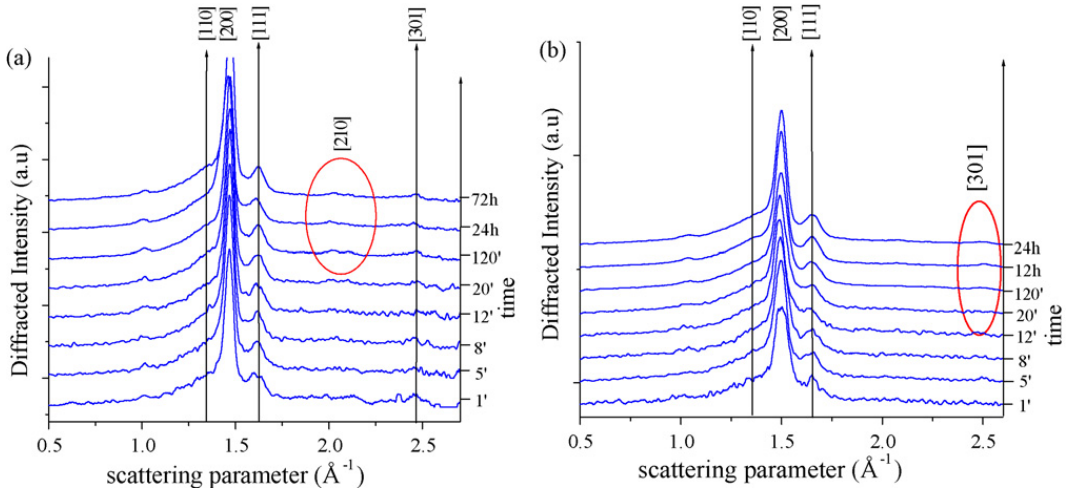

Fig. 6. Highlight of the sequences of EDXD patterns collected during the early stages of crystallization of cement 1 (a) and cement (2).

intensities were plotted as a function of time (Fig. 7B) but, in this case, no variation can be detected, inducing to conclude their characteristic formation times are related to the primary crystallization process ($\tau < 1$–2 s.).

The crystallization process of the other precursor, namely $Ca_4P_2O_9$ powder, as far as it concerns the secondary stage, somehow differs from the previous one. Indeed although, on one hand, also in this case the shape of the pattern collected during the first 60 s can be already attributed to final cement, i.e. the primary crystallization cannot be observed, nevertheless, on the other hand, the final cement exhibits only traces of the [2 1 0] reflection. Therefore, the kinetics of the cementification process can be followed solely monitoring the [3 0 1] Bragg peak evolution (as shown in Fig. 8). The characteristic time of the secondary crystallization in this case is $\tau_2 = (16 \pm 1)$ hours, i.e. slightly less than that of the previous compound.

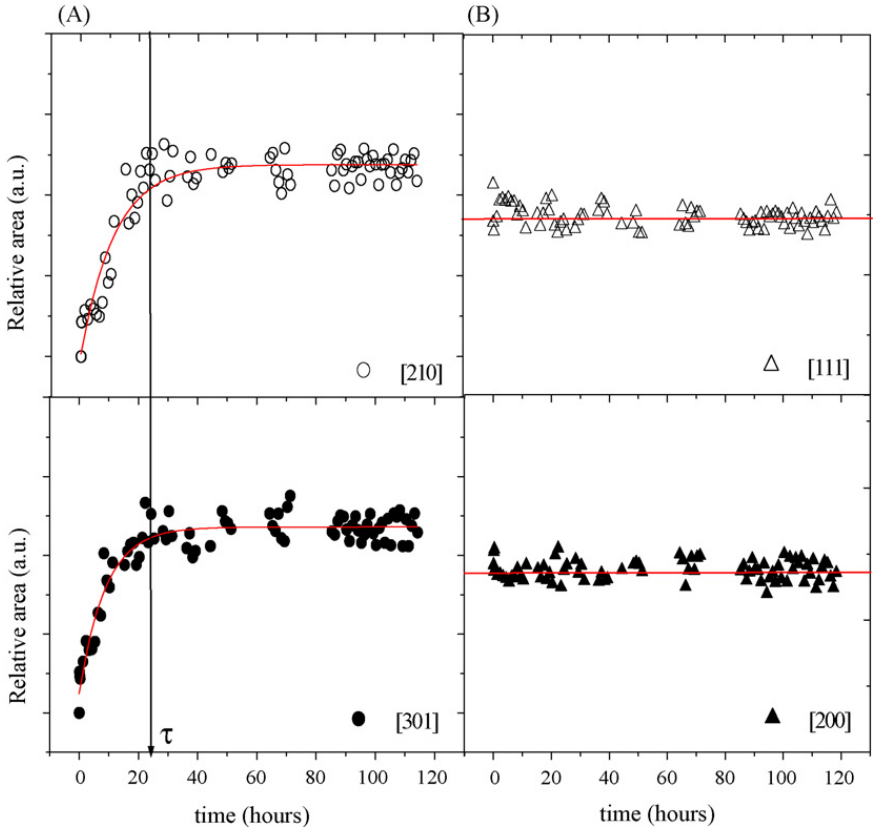

Fig. 7. Precursor powder $Ca_3(PO_4)_2$. The relative intensities of the Bragg peaks as a function of time are related to the primary formation of the cement (A) and the secondary crystallization (B). The characteristic times of the processes are deduced by fitting procedures (black lines).

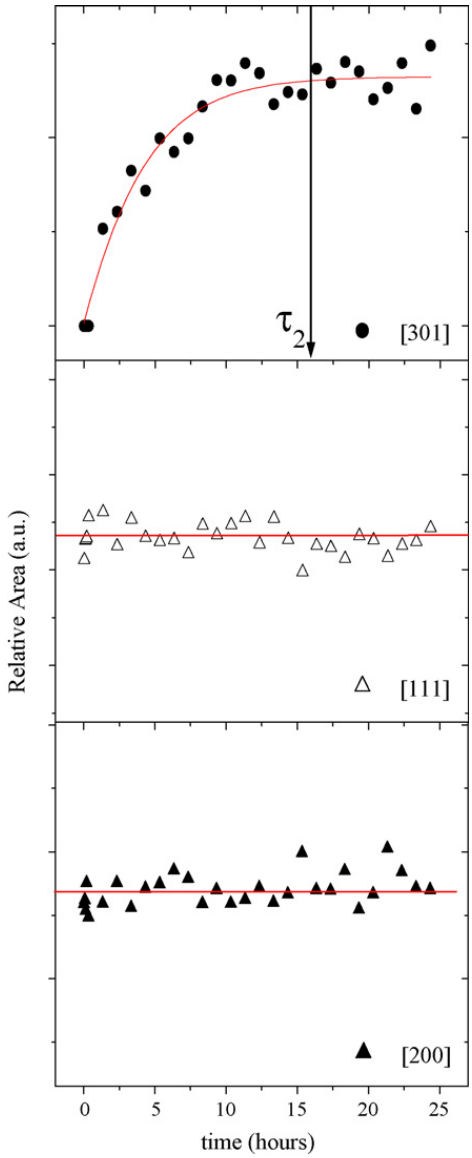

Fig. 8. Precursor powder $Ca_4P_2O_9$. The relative intensities of the Bragg peaks [2 0 0] and [1 1 1] as a function of time are related to the primary formation of the cement. The secondary crystallization process is attributed to the formation of the [3 0 1] reflection and the characteristic time of this process is obtained by the Boltzmann fit.

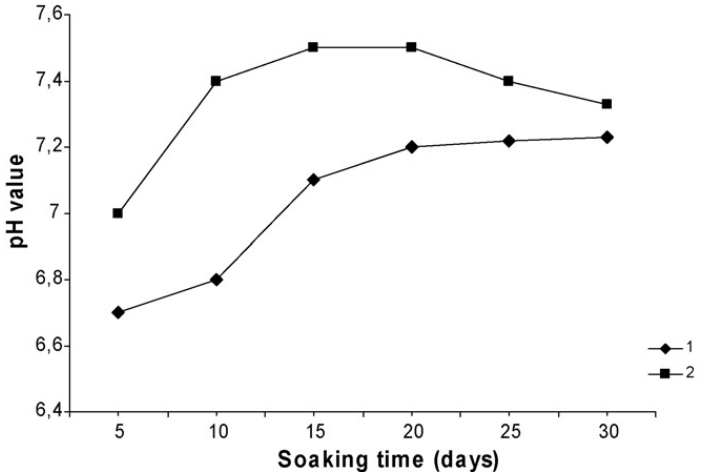

Fig. 9. Dependence of pH value on soaking time for cements 1 and 2.

3.2. Properties of cements

Both cements were set during the period 8–12 min. Density of cements measured by a hydrostatic weighing test was in the range from 2.2 to 2.4 g/cm^3 and open pores content was less than 1%. According to the EDXD data, only the primary crystalline phase in both cements is apatite-like phase. The remaining product of interaction between the powders and the liquids can be attributed to an amorphous phase forming the intergranular material, which is responsible for the adherence of grains resulting in the hardening.

Shown in Fig. 9 is the dependence of pH on the soaking time for both cements. The pH value of 5 days set cements is close to neutral indicating that no significant amount of either soluble acidic (α-TCP, cement 1) or basic (TetCP, cement 2) phase is present in the set cement. Cement 1 is a little more acidic compared to the cement 2. The following interactions

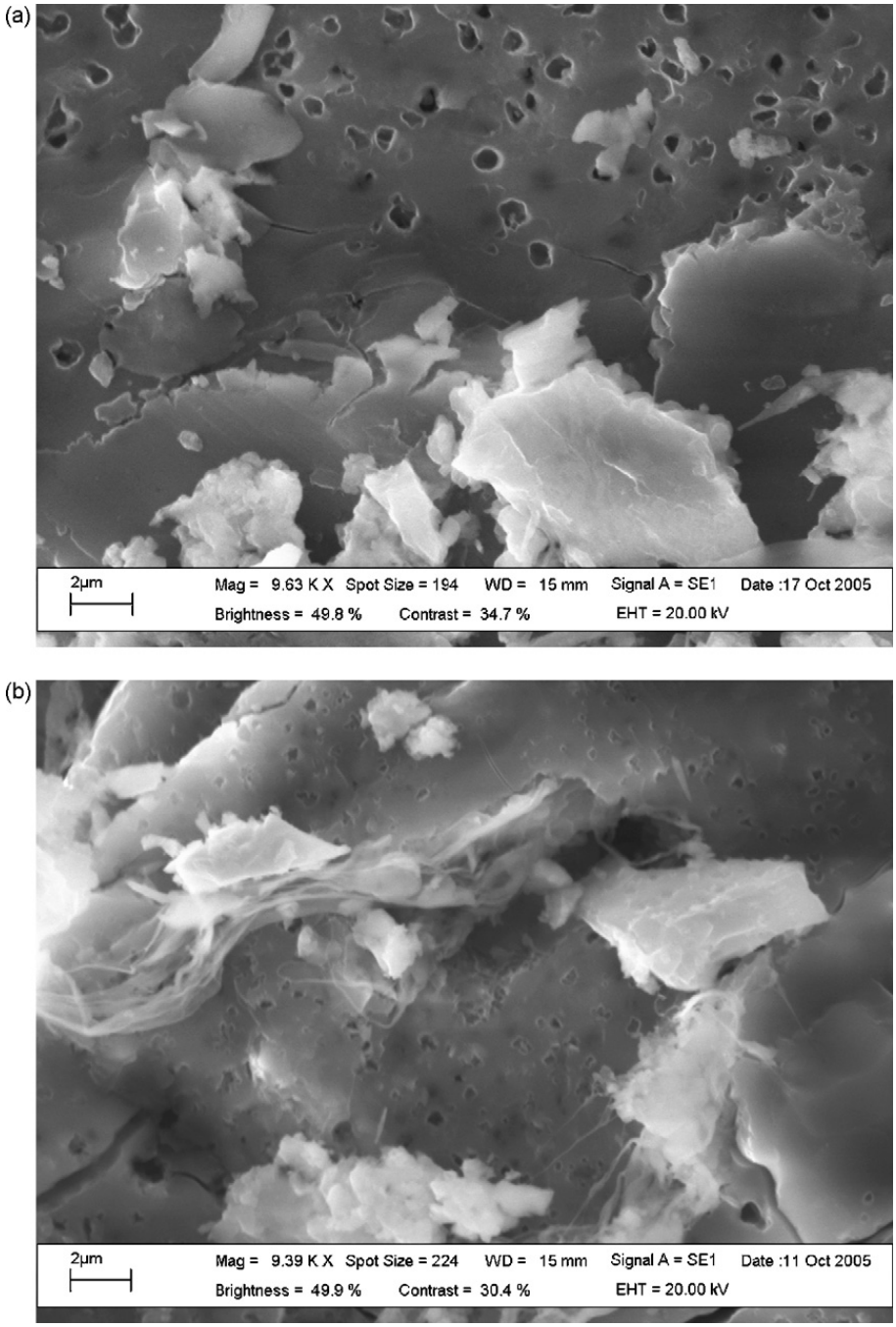

Fig. 10. SEM micrographs of 5-days set cement 1 (a) and cement 2 (b).

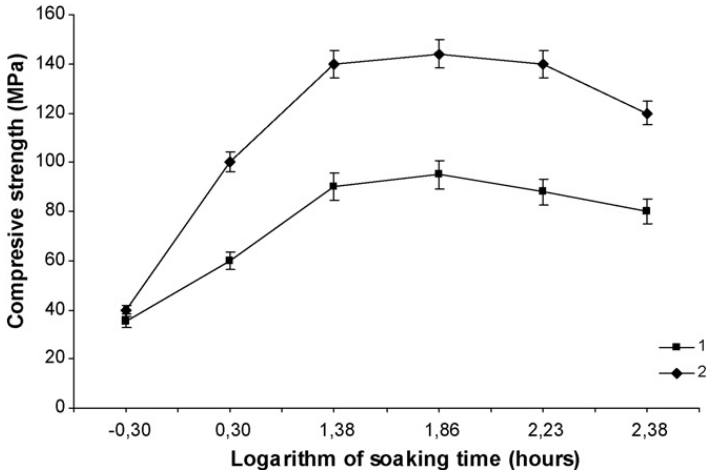

Fig. 11. Effect of soaking time on compressive strength of cements 1 and 2.

could be supposed to describe the setting of the cements. In the cement 1, the initial α-TCP reacts with water of the hardening liquid, resulting in crystallization of a calcium-deficient hydroxyapatite and an amorphous phase [11]: $3Ca_3(PO_4)_2 + H_2O \rightarrow Ca_9(HPO_4)(PO_4)_5(OH)$, whereas the rest of α-TCP interacts with the reaction product between the H_3PO_4 and $MgCO_3$ in the hardening liquid, resulting in the formation of an amorphous magnesium-calcium phosphate as the second phase. The composition of the latter can be close to that of dicalcium(magnesium) phosphate dehydrate, which results in slightly acid pH value. In due of time, this phase can be transformed into apatite in an aqueous solution inducing an increase of pH value to neutral [16]. A qualitative energy-dispersive X-ray analysis on the cement surface revealed both the crystalline and the amorphous phase contain magnesium ions.

In the cement 2, the initial TetCP interacts with phosphorous acid: $5Ca_4P_2O_9 + 2H_3PO_4 \rightarrow 4Ca_5(PO_4)_3(OH) + H_2O$ and, again, an amorphous magnesium-containing calcium phosphate phase can be formed due to the reaction with the product of interaction between phosphoric acid, water and magnesium carbonate in the hardening liquid. The magnesium ions content is sufficiently lower in the liquid for cement 2 than that for cement 1, so this liquid is more acid. As a consequence, the intergranular phase which gives the pH value close to neutral was developed due to the interaction of basic TetCP with acidic liquid. In time the pH of cement 2 trends to neutral value, a maximum resulting from a secondary phase development during the hardening process.

The SEM micrographs of the cements surface are given in Fig. 10. The DAP crystals appear in surrounding non-crystalline matrix for both cements. Fig. 11 shows the compressive strength versus the soaking time. The strength rises with time reaching a maximum at 3 days of hardening due to the microstructure development, particularly the secondary crystallization of the crystalline apatite-like phase and changes occurring in the intergranular phase, followed by a decrease resulting from partial dissolution of the intercrystalline phase. Generally, the strength level of the cements exceeds that for reported by the references [6,12], probably due to the high density of the cements under study.

4. Conclusion

The EDXD method was employed to the study of the phase development during the setting reaction in two different calcium phosphate cement systems based, respectively, on α-TCP and TetCP as solid phase, and magnesium containing phosphoric acid as the hardening liquid. The cement setting reactions in both cements advance without formation of any crystalline other than apatite-like phase. The process of phase development is very fast, being the primary crystallization. The reaction is completed during a few seconds of the setting time followed by a secondary crystallization, characteristic times of this secondary process being of approximately 23 and 16 h for the cements 1 and 2, respectively. Thus, both the strength and the pH development with hardening time in the cements are due to the processes in the second intregranular phase which is X-ray amorphous.

Acknowledgment

The work is supported by the RAS-CNR project agreement and by the RFBR project 06-03-08028.

References

[1] R.Z. LeGeros, Monographs in Oral Surgery, 1, S. Karger, Basel, 1991.
[2] L.L. Hench, J. Wilson, An Introduction to Bioceramics, World Scientific, London, 1993, pp. 8, 146, 331, 335.
[3] F. Theiss, D. Apelt, B. Brand, A. Kutter, K. Zlinzky, M. Bohner, S. Matter, Ch. Frei, J.A. Auer, B. von Rechenberg, Biomaterials 26 (2005) 4383–4394.
[4] W.E. Brown, L.C. Chow, J. Dent. Res. 62 (1983) 672–677.
[5] E. Fernandez, F.J. Gil, M.P. Ginebra, F.C.M. Driessens, J.A. Planell, S.M. Best, J. Mater. Sci. Mater. Med. 10 (1999) 169–183.
[6] M. Bohner, Injury 31 (S) (2000) 37–47.
[7] M. Vallet-Regi, J.M. Gonzalez-Calbet, Progress Solid State Chem. 32 (2004) 1–31.
[8] S.M. Barinov, V.S. Komlev, Calcium Phosphate Based Bioceramics, Science, Moscow, 2005.
[9] M. Bohner, U. Gbureck, J.E. Barralet, Biomaterials 26 (2005) 6423–6429.
[10] R.Z. LeGeros, A. Chohayeb, A. Shulman, J. Dent. Res. 61 (1982) 343–346.
[11] C. Durucan, P.W. Brown, J. Mater. Sci. Mater. Med. 11 (2000) 365–371.
[12] C. Liu, W. Shen, Y. Gu, L. Hu, J. Biomed. Mater. Res. 35 (1997) 75–80.
[13] F. Ronci, B. Scrosati, V. Rossi Albertini, P. Perfetti, Electrochem. Solid State Lett. 3 (2000) 174–177.
[14] F. Ronci, B. Scrosati, V. Rossi Albertini, P. Perfetti, J. Phys. Chem. B 105 (2001) 754–759.
[15] R. Caminiti, V. Rossi Albertini, Int. Rev. Phys. Chem. B 18 (1999) 263–269.
[16] G. Vereecke, J. Lemaitre, J. Cryst. Growth 104 (1990) 820–832.